A work-horse neutron imaging station at the Laboratorio Energia Nucleare Applicata (LENA) in Pavia (Italy): Instrumental components and applications in the frame of the CHNet-NICHE

PAPER • **OPEN ACCESS**

A work-horse neutron imaging station at the Laboratorio Energia Nucleare Applicata (LENA) in Pavia (Italy): Instrumental components and applications in the frame of the CHNet-NICHE INFN experiment.

To cite this article: F Grazzi *et al* 2023 *J. Phys.: Conf. Ser.* **2605** 012006

Journal of Physics: Conference Series **2605** (2023) 012006 doi:10.1088/1742-6596/2605/1/012006

A work-horse neutron imaging station at the Laboratorio Energia Nucleare Applicata (LENA) in Pavia (Italy): Instrumental components and applications in the frame of the CHNet-NICHE INFN experiment.

F Grazzi[1,2], F Cantini[1,2,3], O Sans-Planell[4,5], M Magalini[4,5], L Vigorelli[4,5,6], G Marcucci[7,8], M Clemenza[7,8], M Morigi[9,10], A Re[4,5], D Alloni[11,12], M Prata[11,12], and N Gelli[1]

[1] INFN Sezione di Firenze, Italy
[2] Consiglio Nazionale delle Ricerche, Istituto di Fisica Applicata "Nello Carrara", Sesto
[3] Dipartimento di Fisica e Astronomia, Università degli Studi di Firenze, Italy Fiorentino, Italy
[4] INFN, Sezione di Torino, Torino, Italy
[5] Dipartimento di Fisica, Università degli Studi di Torino, Italy
[6] Dipartimento di Elettronica e Telecomunicazioni, Politecnico di Torino, Italy
[7] INFN Sezione di Milano Bicocca, Milano, Italy
[8] Dipartimento di Fisica "G. Occhialini", Università di Milano Bicocca, Milano, Italy
[9] INFN Sezione di Bologna, Italy
[10] Dipartimento di Fisica ed Astronomia "Augusto Righi", Università di Bologna, Italy
[11] INFN Sezione di Pavia, Italy
[12] Laboratorio Energia Nucleare Applicata (LENA), Pavia, Italy

f.grazzi@ifac.cnr.it

Abstract. In this work, achieved results on the NICHE project (Neutron Imaging in Cultural HEritage) are presented. It fits in the frame of the Cultural Heritage Network (CHNet) of the Italian Nuclear Physics Institute (INFN), and is devoted to the development and usage of a new neutron imaging station on the thermal port of the 250 kW TRIGA Mark-II reactor installed in the Laboratorio Energia Nucleare Applicata (LENA) in Pavia (Italy). The application of neutron radiography to the diagnostic in the cultural heritage field is quite widespread among the research community since it is a non-invasive technique which allows for revealing of the inner structure of the investigated objects, the identification of different materials and their relative spatial distribution with a suitable level of resolution and contrast. We present here the status and progresses within the project: technical characteristics of the beamline and the imaging station component, measuring configuration, possible applications, and examples.

1. Introduction

Neutron imaging represents a powerful method for morphological analysis and characterization of several categories of materials. The method is fully complementary with X-ray Imaging allowing to obtain a different contrast for metal, or for light element such as hydrogen associated with mineralization phases, making possible to evaluate the metal-mineral interface. The improvement in recent years of digital CCD or CMOS cameras sensitivity, dynamic range, and spatial resolution, combined together with the improved sensitivity and light emission yield of neutron detector based on scintillators, allows

for exploiting neutron radiography capabilities even on low power sources. The range of application of neutron radiography to the morphological diagnostic in cultural heritage artefacts is quite wide since it is a non-invasive technique, which allows the identification of different materials and their relative spatial distribution with a reasonable level of contrast and resolution [1, 2].

In this frame, the Cultural Heritage Network (CHNet) [3] of the Italian Nuclear Physics Institute (INFN) proposed and started a project called Neutron Imaging in Cultural HEritage (NICHE) devoted to the development and exercise of a neutron imaging station on the thermal port of the 250 kW TRIGA Mark-II reactor managed by the Laboratorio Energia Nucleare Applicata (LENA) in Pavia.

In this work, we will present the status and operation of the project: technical characteristics of the beamline and the imaging station component, typical measuring configuration, possible applications, and examples.

2. Materials and methods

The NICHE experiment established a neutron imaging station at the TRIGA reactor of LENA on the thermal beam port channel B [4]. The experiment is funded by INFN as part of its applied physics program. NICHE works as a neutron imaging station and was established in April 2021, running for the equivalent of 30 beam-time days so far, since the beamline is shared with other activities. The components are easy to remove and install and the set-up takes about 2 hours.

Beam port B is the one among the TRIGA available ports, exhibiting the highest ratio between thermal and higher energy neutrons and thus presenting the best potential for imaging applications with thermal neutrons [5, 6]. The flight tube, located between the reactor core and the experimental hutch includes several filtering elements, such as a 70 mm bismuth and a 100 mm sapphire layers, to lower the flux of non-thermal neutron and gamma ray. The Monte Carlo N-Particle 6 [7] simulated the flux at the shutter beam position including the effect of the filtering elements. The obtained value is 7.0×10^6 $cm^{-2}s^{-1}$ for the thermal component, 9.3×10^4 $cm^{-2}s^{-1}$ for the epithermal component, and 4.1×10^4 $cm^{-2}s^{-1}$ for the fast component. The evaluated gamma flux is about 10^5 $cm^{-2}s^{-1}$ MeV^{-1} in the range 1-5 MeV [5]. The main components of the NICHE station are described in the following. The instrument is equipped as described below.

1) A double layer shutter pneumatically controlled from outside the experimental hutch.
2) A pin-hole selector with manually interchangeable B_4C ceramix [8] cartridges with pin-hole diameter 10, 20 and 30 mm, encapsulated within an aluminium holder and a Polylactic Acid (PLA) 3D printed frame.
3) An experimental hutch, whose main area is 2500 mm length, 600 mm width, 2100 mm height, accessed with double corner entrance area. It is equipped with a set of three guide rails collinear with the neutron beam and connected to the sample holder and the neutron camera box, making possible to adjust the L/D collimation power and the neutron flux on the sample.
4) A custom-made sample positioning area, equipped with two remotely controlled motorized linear stages along the vertical direction (z-axis, stepper-motor based system) and the horizontal direction perpendicular to the beam (x-axis, stepper-motor based system) allowing to move samples in and out the beam and remotely allow fine sample alignment. Those two motors are controlled through a single Arduino Mega and LD09 CNC driver. A third remotely controlled vertical axis rotating stage (ω-axis, Physik Instrumente, PI) allows for sample rotation and potential tomographic projection acquisition. The typical working distance between sample axis and the detector, taking into account the encumbrance of the various components, is of the order of 40 mm. All the motors are controlled via a LabView 2018 SP1 developed code, described in the following section, which also includes the acquisition control of the neutron camera.
5) A custom-made neutron dark camera box containing an Ag doped 300 μm thickness ^{6}LiF/ZnS 2:1 composition ratio scintillator screen produced by Tritec, and coupled with a ZWO ASI 2600 MM CMOS monochromatic digital camera (16 bit) double Peltier air cooled, through a f/1.6, 35 mm optic lens, mounted on a remotely controlled translation stage. The projection of a camera pixel on the scintillator corresponds to an area 30 μm x 30 μm and the available field of view of such an

optic configuration is 180 mm (horizontal) x 120 mm (vertical). The scintillator thickness choice was made by comparing the efficiency and light yield of a set of test scintillators of different thickness and mixture, also provided by Tritec, and selecting the value at which the linear increase of the intensity began to decline.

A scheme of the NICHE set-up inside of the experimental hutch is shown in figure 1.

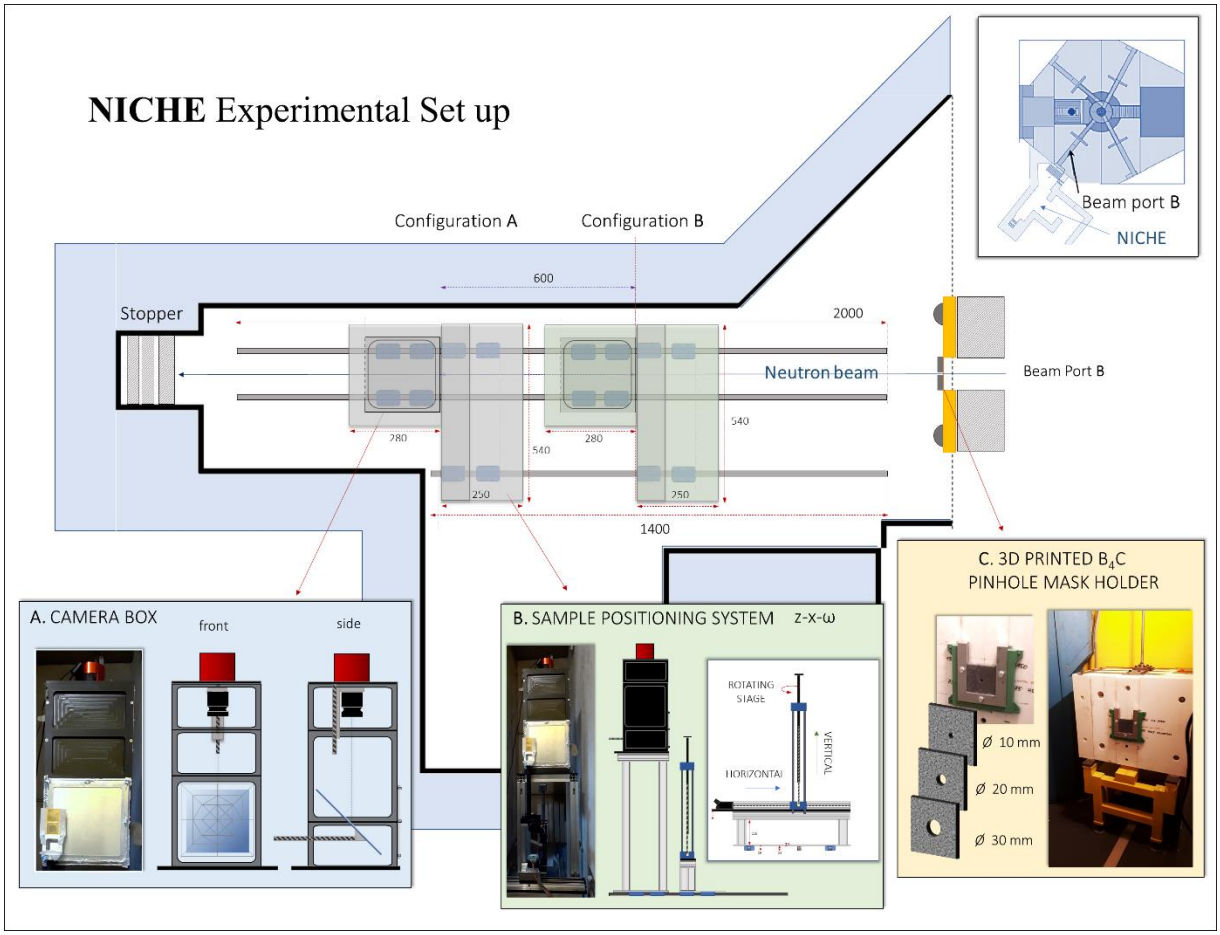

Figure 1. Top view of the experimental hutch built around beam port B where the NICHE experiment is set. The main diagram shows two configuration *A*, and *B*, for high resolution or high flux measurement respectively. Both the camera box and the sample stage can slide on guide rails to easily adjust the L/D collimation power. Panel (**A**): Camera Box system scheme showing the arrangement of the inner components: the scintillator screen, the 45° oriented mirror to move the light emitted by the scintillator out of the neutron beam, the focusing lens and the CMOS camera. Panel (**B**): a scheme showing the sample positioning system, equipped with two stepper motors (horizontal and vertical translation) and a PI rotating stage. Panel (**C**): PLA 3D printed B_4C+ ceramic-based [8] pinhole mask Holder and 3 mask with a pin-hole aperture of 10 mm, 20 mm, and 30 mm.

Due to the combined effect of the shape and size of the experimental hutch and sample positioning system, which needs to safely move the sample out of the primary beam, there are limitations in the relative distance of the camera and the sample holder with respect to the beam shutter and pin-hole system. The distance value between the shutter and the scintillator ranges between 1100 and 1920 mm, thus determining a minimum and maximum nominal value for the L/D coefficient (pin-hole diameter 10 mm) of 110 and 190 respectively. Due to the round shape of the pin-hole, the beam shape is a circle with diameter increasing with distance, due to beam divergence. We decided to not install beam limiters since the beam profile at the exit of the port B is reasonably collimated and there is no penumbra over a

diameter 150 mm wide at 1920 mm distance from the shutter. In order to evaluate the ideal acquisition time at different distances, we performed several tests to verify the linear response to light intensity on the camera, and decided to set the maximum intensity at 75% of the full scale (48000 counts per pixel). Considering as almost negligible the intrinsic and read-out noise generated by the CMOS system, we set the acquisition time accordingly. Resolution was measured using a method based on the direct observation of lines tacking in to account the 30% contrast variation, exploiting the two devices released by the Paul Scherrer Institut, namely the "bar pattern" and the "Siemens star" [9]. The resolution was measured with the devices directly stick on the scintillator (this configuration was also used to optimise the 35 mm lens focusing distance from the camera) and at a typical working distance to perform radiographies and tomographies of samples in good size proportion with the available field of view (40 mm).

The two set-up at minimum and maximum distance provide the highest possible flux and the highest resolution respectively. Anyway, the most used setting is an average one, whose details are summarized in table 1.

Table 1. Average instrumental and dimensional parameters of the configuration of the NICHE station imaging set-up. All values are reported considering the 10 mm pin-hole diameter.

Parameter	Value
Pin-hole to scintillator distance	1410 mm
Thermal neutron flux at sample position	$2E^5$ $cm^{-2}s^{-1}$
L/D coefficient	140
Field of view (round section)	65 mm
Field of view (maximum square)	45 x 45 mm
Best spatial resolution (0 mm distance from scintillator)	150 μm
Working-distance spatial resolution (40 mm distance from scintillator)	180 μm
Best signal to noise acquisition time	1200 s
Usual acquisition time	600 s
Tomography-mode acquisition time	150 s

Since the spatial resolution is more than a factor two lower than the pixel size (30 μm), it is reasonable to adopt 2x2 average binning on data directly on the camera acquisition mode to increase signal to noise ratio, before normalization process takes place. We verified there is no spatial resolution degradation induced by the binning.

The reason why tomography acquisition time was set to 150 s is due to the working procedure of the TRIGA reactor. The current status allows for two shifts 3.5 hours long (morning and afternoon) every day from Monday to Thursday, so that daily operation time is, at maximum, 6.5 hours (excluding sudden stops and service activity). An average number of 300 projections for a tomography is a good compromise between resolution, horizontal pixel distribution along the field of view, and available beam-time, so that a tomography can be completed in 2 operational days, including white beam and dark current ancillary measurements.

2.1. Software and control system description.

As mentioned in the section above, the custom-built control software designed for the NICHE set-up is programmed in the LabView 2018 SP1 environment. In order to develop a flexible, state-of-the-art facility from the software and user interface perspective, the architecture employed was an event-driven producer/consumer master program, with several slave programs which independently control different aspects of the hardware (namely, the Arduino-controlled motors, the PI rotary stage, and the camera, with flexibility to include any number of extra components). Each slave program is built upon a template state machine, from which simple commands are executed when the user interacts with the program interface, or a specific routine is launched (e.g. a tomography). At present status, 3 slave programs allow respectively:

- to move the 3 linear stage motors (x-z sample translation and camera focusing) independently. Positions can be saved and retrieved from a file for executing sequences of radiographies in different areas of the sample;
- to control the PI rotary stage (rotation step, offset angle, total rotation angle);
- to set the acquisition parameters for the ZWO ASI camera (e.g. exposure time, gain, cooling system status) and start an acquisition.

This kind of architecture is ideal for a test beamline, as it allows the freedom to independently debug single components of the sample movement and acquisition system, while allowing for a wide control of all the variables involved. The set-up can be controlled remotely and has been used in tandem with complex external hardware elements, such as a PI hexapod. Finally, through a custom Python 3 routine executed within LabView, the acquired images are saved in FITS format, which allow also to store all the useful variables involved in a single radiograph as camera exposure time, temperature, power, PI motor position, set-up position, Arduino status.

3. Neutron imaging test examples

In this section, we report some examples of neutron radiographies and tomographies performed at the NICHE station. All the shown data were acquired at 1400 mm detector distance from the pin-hole. Data were normalized applying the same procedure for all of them: they were processed using ImageJ software [10] performing, at first, the remove outliers filtering, 2x2 average binning and then combining the radiographic images with open beam (OB) and dark current (DC) images (filtered and binned in the same way) for normalization purposes according to the relation:

$$I_{norm} = \frac{I_{sample} - I_{DC}}{I_{OB} - I_{DC}}. \quad (1)$$

If not differently indicated, radiographies were taken at 300 s acquisition time, while tomographic projections were taken at 150 s acquisition time. Resolution measurements were performed by exploiting the radial lines of the Siemens star and the Bar pattern devices [9], positioned at different distances from the scintillator surface, at 0 mm and at 40 mm distance. Examples are shown in figure 2.

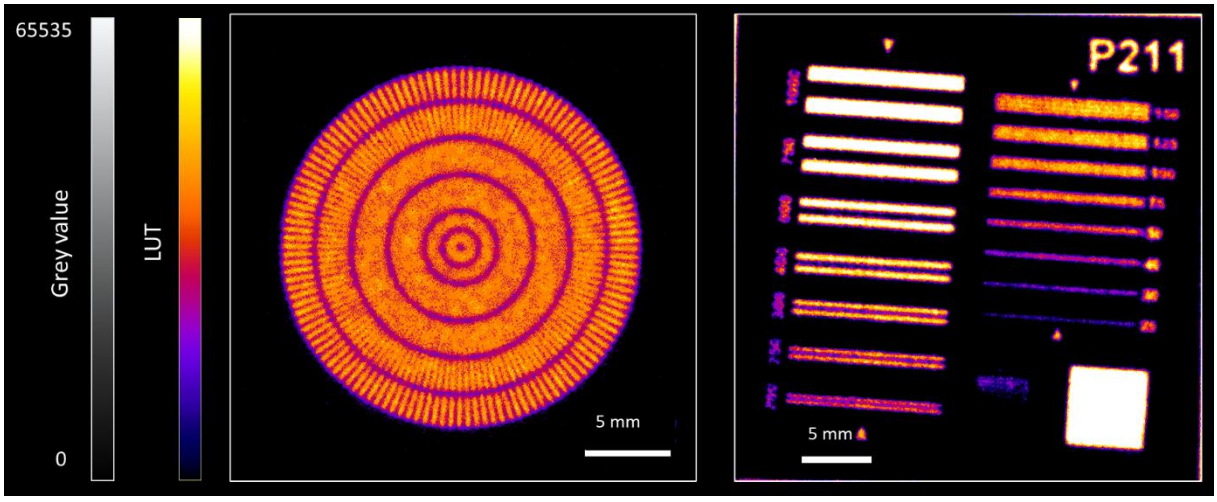

Figure 2. Neutron radiography of the PSI Siemens star and bar pattern to determine resolution at different sample to scintillator distances. Integration time 600 s. Left image: sample-scintillator distance 0 mm, interpolated resolution 150 µm. Right image: sample-scintillator distance 40 mm, interpolated resolution 180 µm. Neutron Radiographies are shown here using a false colour scale (Look Up Table FIRE, ImageJ) to enhance readability.

In order to verify the potential of the imaging station we performed several test radiographies, rocking curves and tomographies on a wide range of samples, containing materials able to provide good contrast thanks to neutron scattering or absorption by the nuclei. In figure 3 **(A**, **B**, **C**), we report a set of samples containing thin high scattering elements (metal wires), low scattering vessels (glass, aluminium case), high incoherent scattering case (plastic polymer) and high-absorption / high-scattering composite components (Li-polymers). All these elements exhibit a reasonable resolution and contrast to be morphologically and spatially evaluated. Figure 3 (**D)** shows the potential use of a mosaic reconstruction of a set of neutron radiographs taken on a medium size sample with respect to the available field of view. The image stitching, performed using ImageJ plugin [11], shows good homogeneity and makes the resulting image readable for analytical purposes. In figure 4 and 5, it is shown the analysis of a purposely built sample to verify sensitivity and resolution characteristics of the imaging station respect to thick samples. By exploiting the remotely - controlled rotating stage, we took radiographs at different orientation angles (step 0.5°) of a composite sample, constituted by three layers planar structure, made of aluminium (8 mm thick), copper (0.2 mm thick), aluminium (8 mm thick). The measurements show the projection of the copper sheet in the radiographies, considering its relative orientation.

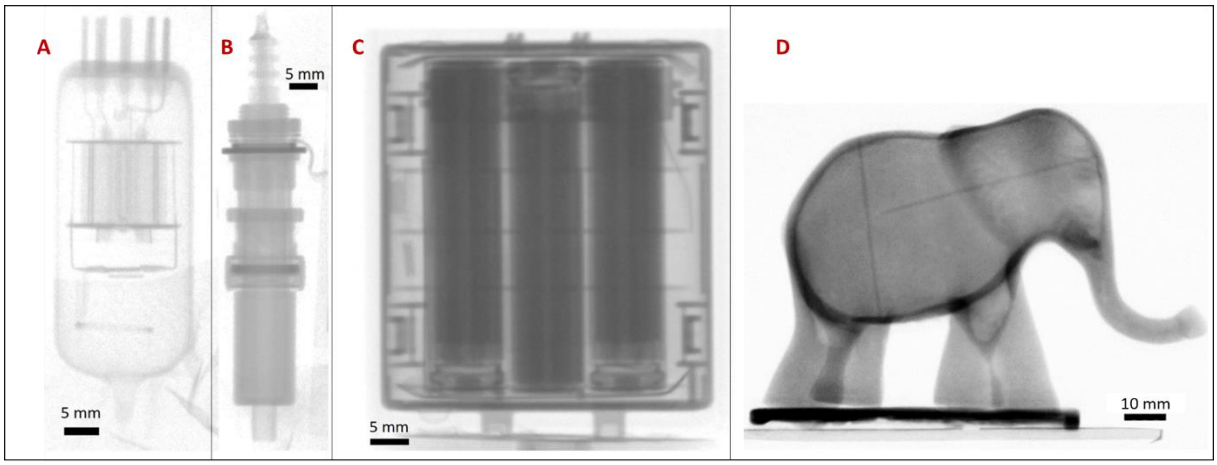

Figure 3. Neutron radiography on samples of different materials: a thermionic valve (**A**); a Bayonet Neill–Concelman (BNC) connector (**B**); and a Li ion battery (**C**). Samples (**A**), (**B**), and (**C**) were placed as close as possible to the scintillator, on an average distance of 10 mm. and they show a good resolution and contrast nevertheless the thin metal wires. On the right in the figure (**D**) the neutron radiography of a modern bronze statue of an elephant produced in China. The image is the result of the stitching of a set of 4 neutron radiographies taken at four positions at the corners of a square, horizontally-and vertically shifting the sample 30 mm. Stitching was applied after binning and normalization procedure using the ImageJ plug-in [11]. Sample - scintillator distance 40 mm.

The transmittance profile and FWHM are represented in figure 5, showing how a thick sample (40 mm along beam direction) generates a blurring effect which is a factor 2 larger than the resolution but its projection is anyway minimized when the sample is aligned with the beam.

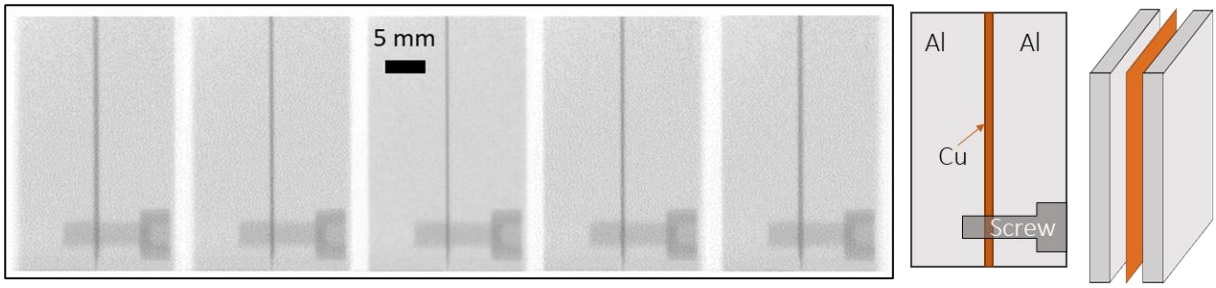

Figure 4. Selected radiographies of an angular scan of 51 images taken at 0.5 degrees step, showing images of an aluminium two valves support containing a copper foil 200 μm thickness in between, scheme reported on the right. The figure shows 5 pictures taken at 0.5° step one another, with the central one exhibiting the thinnest Cu foil image. Integration time for each image 150 s, sample axis - scintillator distance 40 mm, pixel size binned to 90 μm.

Thanks to the possibility to prepare scripts able to combine sample motion with image acquisition, we were able to perform some tomographies in which we were forced to set the acquisition time and the number of projections with the reactor daily cycles (3.5 hours in the morning and 3.5 hours in the afternoon). We then set a tomography to 150 s acquisition time and 300 projections, corresponding to around 12 hours work, including readout time and motor adjustments. In this way it becomes possible to perform a tomography in 2 days. Data treatment was performed using ImageJ [10] for filtering and normalization and Octopus Reconstruction [12] for obtaining tomographic slices. Data were then average binned a factor 2 and 3D rendering was performed using 3D Slicer [13]. In order to maximize the imaging production output in a limited time, we filled up the field of view (FOV) by including as many samples as possible, avoiding that any samples went out of FOV during rotation.

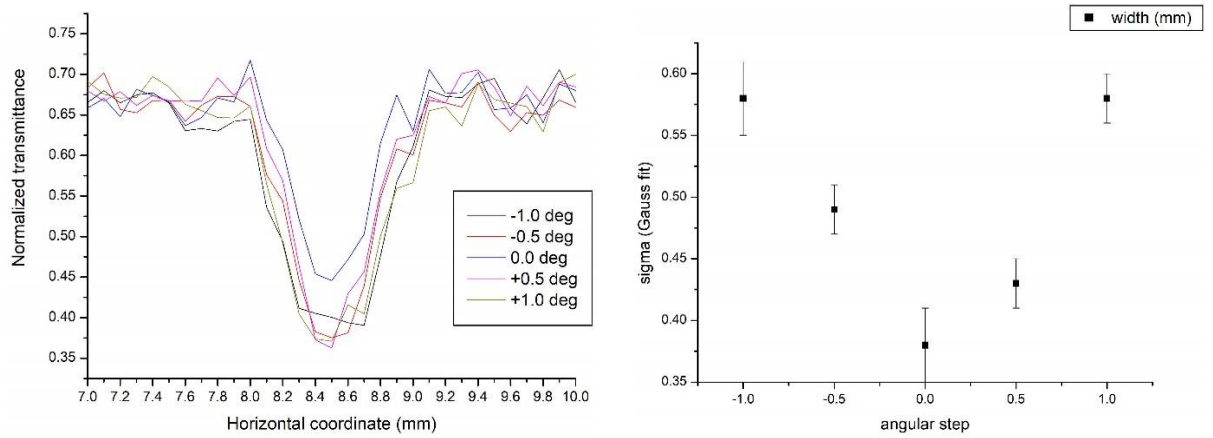

Figure 5. Left: Transmittance profile crossing the composite system including two external Al walls surrounding Cu foil at different orientation angles. Analysis results show the width of the attenuation effect of copper as a function of the orientation respect to the beam. Right: value of sigma full width of the Gaussian fit of the transmittance profile as a function of the tilt angle.

A test tomography measurement allowed us to verify the sensitivity of the instrument to different metal alloys and plastic. The measurement was performed using an aluminium drum with five cylindrical holes, arranged on the vertexes of a regular pentagon, and filled with seven small cylinders made of different materials. The sample and the tomography results are shown in figure 6. The attenuation coefficients of the various elements and composites are significantly different. Polyethylene and silver cylinders show some differentiated attenuation effects, which can be ascribed to scattering and absorption beam hardening respectively. They can be dealt with during tomographic reconstruction of such elements alone, applying specific corrections.

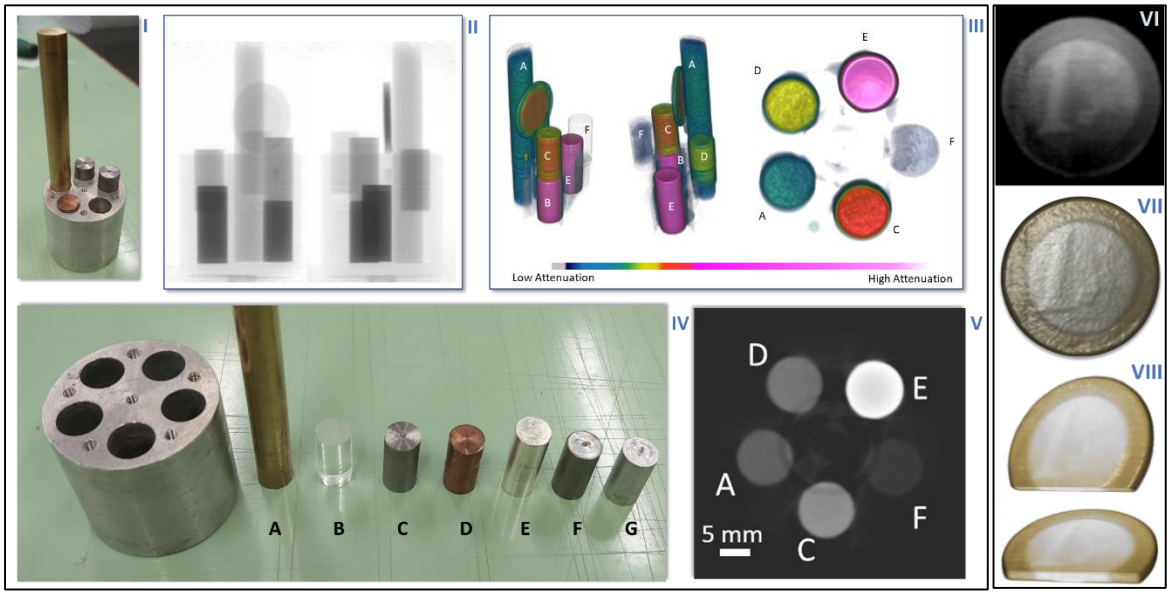

Figure 6. **I**) Photograph of the composite sample consisting in a drum filled with cylinders made of seven different materials, some samples are superimposed, one on top of another. **II**) Selected projections during the data acquisition process. **III**) False colour 3D rendering of the different cylinders, showing different attenuation coefficients. Materials are A: brass; B: polyethylene; C: iron; D: copper; E: silver; F: lead; G: aluminium. **IV**) Picture of the components. **V**) Tomographic slice showing the different attenuation coefficients. Silver sample (E, high-absorption cross section) shows beam-hardening effect to be corrected through data treatment. **VI), VII), VIII**) Tomographic slice and 3D rendering images (integer and sections) of a 1 Euro coin. It is possible to see the different attenuation coefficient of the Nordic gold alloy (Cu-Zn as main elements) of the external crown respect to the Ni-based alloy central volume of the coin.

Together with the drum and element cylinders, a 1 Euro coin was also measured (it can be observed in Fig. 6 III) and, despite the low number of voxels describing the sample volume, it is possible to observe the different attenuation of the external (Nordic gold) and central (Ni based alloy) metal as well as the surface morphology, shown in figure 6 (VI – VIII).

Tomographic slices and 3D rendering of a plastic figure is shown in figure 7. The sample size is 40 mm height, and the inner features are well visualized within the NICHE resolution range. Notwithstanding plastic is a high scattering compound because of its high hydrogen content, the constructive details are well defined and inner and outer surfaces can be mapped.

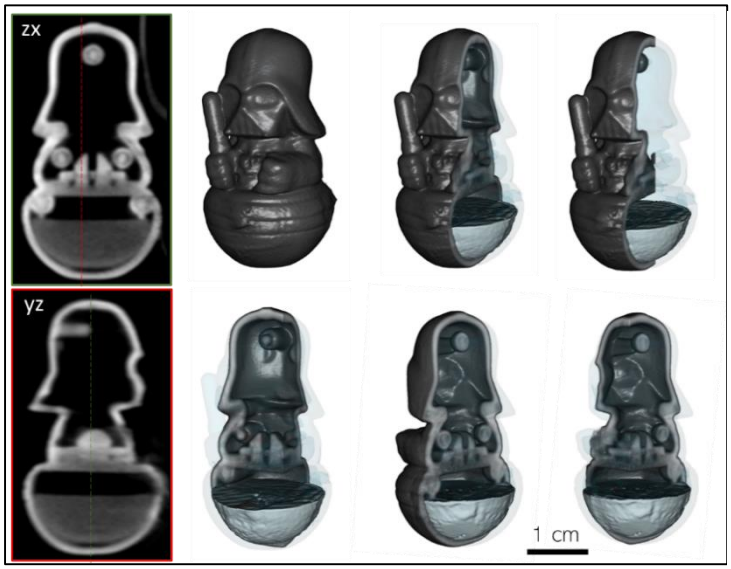

Figure 7. On the left side of the picture tomographic slices along zx and yz planes and 3D rendering and sectioning of a 40 mm height plastic figure, containing magnetite hemisphere in the basement. The construction details are clearly shown as well as the regular thickness and density of the plastic. Despite the high scattering power of hydrogen, the image appears well defined.

4. Conclusion

The CHNet-NICHE thermal neutron imaging station has been installed and is operational at the TRIGA reactor of the Laboratorio Energia Nucleare Applicata, Università di Pavia. It shows good capabilities to perform neutron radiography and neutron tomography on a field of view of 45x45 mm. The station will be made available in the frame of the CHNet Cultural Heritage Network providing access to advanced diagnostic techniques to cultural heritage stakeholders. Rail-based motion system and LabView based remote control software allow users to get high flexibility to perform radiographic scan and tomography also on complex sets of samples thus optimizing the limited beam operation time of the facility.

Acknowledgements

The INFN 5th committee and the CHNet INFN network are gratefully acknowledged for the technical and economic support to the development of this activity. The whole CHNet-NICHE collaboration is acknowledged considering the different capabilities devoted to the development of the project. The contribution of Dr. Burkhard Schillinger from MLZ and Dr. Nikolay Kardjilov from HZB are also acknowledged for the suggestions on the choice of the instrumental components.

References

[1] Kardjilov N, & Festa G (Eds.) 2017. *Neutron methods for archaeology and cultural heritage* (p. 349). Berlin: Springer.
[2] Lehmann E H, Deschler-Erb E and Ford A 2010 *Archaeometry* **52** 272-285.
[3] Giuntini L, Castelli L, Massi M, Fedi M, Czelusniak C, Gelli N, … and Taccetti F 2021 *Applied Sciences* **11** 3462.
[4] Grazzi F, Cantini F, Gelli N 2022 *International Neutron Radiography Newsletter* **17** 9-11 https://www.isnr.de/images/nr_newsletter/NR17.pdf
[5] Salvini A, Alloni D, Altieri S, Protti N, and Clemenza M 2020 *Research Reactors: Addressing Challenges and Opportunities to Ensure Effectiveness and Sustainability. Summary of an International Conference.* Supplementary Files.
[6] Prata M, Alloni D, De Felice P, Palomba M, Pietropaolo A, Pillon, M, ... and Valente P 2014 *The European Physical Journal Plus* **129** 1-15.
[7] Werner C J, Bull J S, Solomon C J, Brown F B, McKinney G W, Rising M E, ... and Zukaitis A 2018 *report LA-UR-18-20808*. Los Alamos National Laboratory, **43**.

[8] Celli M, Grazzi F, and Zoppi M 2006 *Nuclear Instruments and Methods in Physics Research Section A: Accelerators, Spectrometers, Detectors and Associated Equipment* **565** 861-863
[9] Kaestner A P, Kis Z, Radebe M J, Mannes D, Hovind J, Grünzweig, C, ... and Lehmann E H 2017 *Physics Procedia* **88** 258-265.
[10] Abràmoff M D, Magalhães P J and Ram S J 2004 *Biophotonics international* **11** 36-42.
[11] Preibisch S, Saalfeld S, and Tomancak P 2009 *Bioinformatics* **25** 1463-1465.
[12] Dierick M, Masschaele and Van Hoorebeke L 2004 *Measurement Science and Technology*, **15**, 1366.
[13] Uday P A, Digvijay N and Jeeva J B 2014 *2014 international Conference on green computing communication and electrical engineering (ICGCCEE)* 1-4 IEEE.